HHS Public Access

Author manuscript

ACS Appl Mater Interfaces. Author manuscript; available in PMC 2017 August 30.

Published in final edited form as:

ACS Appl Mater Interfaces. 2017 April 26; 9(16): 14422–14428. doi:10.1021/acsami.7b02759.

Light-Stimulated Permanent Shape Reconfiguration in Cross-Linked Polymer Microparticles

Lewis Michael Cox[*,†,‡,⊥], **Xiaohao Sun**[†,§], **Chen Wang**[‡], **Nancy Sowan**[‡,∥], **Jason P. Killgore**[⊥], **Rong Long**[†], **Heng-An Wu**[§], **Christopher N. Bowman**[‡,∥], and **Yifu Ding**[*,†,∥]

[†]Department of Mechanical Engineering, University of Colorado, Boulder, Colorado 80309-0427, United States

[‡]Department of Chemical and Biological Engineering, University of Colorado, Boulder, Colorado 80309-0596, United States

[§]CAS Key Laboratory of Mechanical Behavior and Design of Materials, Department of Modern Mechanics, University of Science and Technology of China, Hefei, Anhui 230027, China

[∥]Material Science and Engineering Program, University of Colorado, Boulder, Colorado 80309-0596, United States

[⊥]Applied Chemicals and Materials Division, National Institute of Standards and Technology, Boulder, Colorado 80305, United States

Abstract

Reconfiguring the permanent shape of elastomeric microparticles has been impossible due to the incapability of plastic deformation in these materials. To address this limitation, we synthesize the first instance of microparticles comprising a covalent adaptable network (CAN). CANs are cross-linked polymer networks capable of reconfiguring their network topology, enabling stress relaxation and shape changing behaviors, and reversible addition–fragmentation chain transfer (RAFT) is the corresponding dynamic chemistry used in this work to enable CAN-based microparticles. Using nanoimprint lithography to apply controllable deformations we demonstrate that upon light stimulation microparticles are able to reconfigure their shape to permanently fix large aspect ratios and nanoscale surface topographies.

Graphical abstract

[*]**Corresponding Authors:** lewis.cox@nist.gov, yifu.ding@colorado.edu.

Supporting Information

The Supporting Information is available free of charge on the ACS Publications website at DOI: 10.1021/acsami.7b02759. Additional experimental data, including AFM experiments, dynamic mechanical analysis testing procedure, finite element simulation details, and deformation of particles during SEM (PDF)

ORCID

Lewis Michael Cox: 0000-0002-5830-3819

Chen Wang: 0000-0003-0985-3221

Notes

The authors declare no competing financial interest.

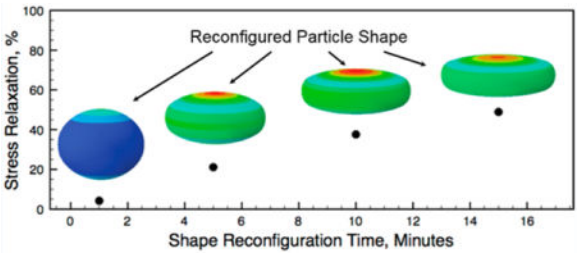

Keywords

microparticles; shape reconfiguration; covalent adaptive network; photoplasticity; smart particles

INTRODUCTION

Polymer micro- and nanoparticles serve as building blocks for photonic devices,[1,2] drug carriers,[3,4] and modifiers of fluids and solids.[5–7] Significant progress has been made in controlling their chemical composition and structural characteristics;[8–10] however, for many if not all of these applications, particle size and shape are crucial design factors. Polymer microspheres are prime candidates for encapsulation and delivery of vaccine adjuvants and antigens, where size and shape are key variables in controlling not only the internalization process but also the cellular and humoral responses.[11] In a comparison with particle size, the importance of particle shape for these applications is only now starting to gain recognition, and in contrast to particle size, control of particle shape has remained a significantly more difficult problem to address.

Particles that change shape as needed are advantageous. To date, two approaches have been reported for solventless, stimuli-responsive particle morphing. Particles made of a liquid-crystalline polymer are able to switch between spherical and elliptical shapes in response to changes in temperature that control the ordering and disordering of mesogens within the particles.[12] However, the magnitude of the shape change achieved is small. More recently, significant shape changes were achieved by using the shape-memory effect in particles.[13,14] The as-synthesized microspheres were either stretched into ellipsoidal shapes when embedded in another polymer matrix or directly compressed into disc-like shapes using a nanoimprinting process, both at temperatures above the glass transition temperature (T_g) of the polymer. These nonspherical shapes were temporarily fixed upon cooling below T_g in their morphed shape, but recovery of the permanent spherical shape occurs upon heating or exposure to favorable solvents.

Recent advances in polymer science have led to a class of novel polymer networks that are capable of relaxing internal stress by breaking and reforming network bonds. This change of network topology allows for reconfiguration of permanent shapes without altering mechanical properties or chemical composition.[15–17] These so-called covalent adaptable networks (CAN) possess the properties of malleability,[18] recyclability,[19] and self-healing,[20] all of which are difficult or impossible for conventionally cross-linked polymers. The corresponding dynamic chemistries that enable these CANs include Diels–Alder,[21,22]

disulfides,[23,24] transesterification,[18] reversible addition–fragmentation chain transfer (RAFT) reactions,[25–32] and recently a one-step nitroxide-mediated polymerization.[33] These dynamic chemistries are triggered by various external stimuli such as heat[18] or light.[25] Light-induced reconfiguration in RAFT-based CANs is particularly attractive because it enables precise spatial and temporal control over the network rearrangement process.[34] Here, we incorporate RAFT-chemistry into polymer microspheres and use UV-based nanoimprint lithography (UV-NIL) to demonstrate large-degree, permanent shape reconfiguration for the first time. Spherical particles are successfully reconfigured into a series of oblate ellipsoids with varying aspect ratios and altered surface topographies.

RESULTS AND DISCUSSION

Figure 1 describes the chemical compositions of the network and illustrates the corresponding RAFT-based bond-exchange mechanism. As detailed in the Materials and Methods section, the RAFT-based microspheres (Figure 1a) were synthesized using a solution-based polymerization process, based on the base-catalyzed thiol-Michael “click” reaction with a 1:1 stoichiometric ratio of thiol to acrylate functional groups. The thiol used was pentaerythritol tetrakis(3-mercaptopropionate) (PETMP), and the two different acrylates used were tetra-(ethylene glycol) diacrylate (TEGDA) and diacrylate (2-methylene-propane-1,3-bis(thioethyl acrylate) (MBTA) (Figure 1c). MBTA was the RAFT-agent and was synthesized according to the literature.[34] The molar ratio of the acrylate groups between TEGDA and MBTA was fixed at 1:1. The thiol-Michael addition polymerization was catalyzed using a mass fraction of 0.6% triethylamine while the subsequent network rearrangement was mediated by the RAFT moiety initiated using Irgacure 651 (dimethoxy diphenyl acetophenone) as a radical generating photoinitiator. The diameter of as-synthesized, unswollen CANs particles was 3.1 ± 0.3 μm (which henceforth represents average ± standard deviation, $N = 30$), according to atomic force microscopy (AFM) measurements. A histogram detailing particle size distribution can be found in Figure S1. This narrow polydispersity is consistent with previous step-growth thiol-Michael dispersion polymerization results.[35,36]

Figure 1b illustrates the photoinduced network rearrangement process in our CAN particles. Upon irradiation with UV light, the initiators dissociate into free radicals where the radicals then react with the RAFT-agent (allyl sulfide groups in MBTA, Figure 1c) to cause bond rearrangement throughout the network. This process causes one network connection to break and a new one to form, while also regenerating a radical. The regenerated radicals react with additional allyl sulfide groups through a reaction-diffusion type process using the RAFT reaction to cause bond exchange throughout the network. Through such repeated cleavage and reformation of the polymer backbones, the network topology undergoes rearrangement, during which the internal stresses are relaxed. At the macroscopic level, the sample is permanently deformed, but the overall network cross-linking density remains unchanged.

We first characterized the thermo-mechanical properties of individual CAN particles with an AFM-indentation measurement. As shown in Figure 1d, we fit the force–displacement curve with a JKR model which shows good agreement. Contact models other than JKR were also employed but were unable to fit the experimental data satisfactorily (Figure S2). The elastic

modulus of the CAN particles at room temperature was calculated to be 12 ± 1 MPa (see Materials and Methods section for detailed discussion), suggesting that the particles are rubbery and the T_g is well below room temperature. To verify this T_g value further, we prepared bulk polymer films with a monomer composition similar to that of the CAN particles. From dynamic mechanical analysis (DMA) measurements (Figure S3), the T_g of the as-prepared CAN film was −15 °C, and the room-temperature modulus was 5 MPa, which agrees well with the AFM measurements on the CAN particles. These measurements confirm that the CAN particles are rubbery throughout the shape-reconfiguring conditions used in this study. Accordingly, no shape-memory effect is present, and any changes in particle geometry are permanent.

The particle shape-reconfiguration process was carried out using a UV nanoimprint lithography (UV-NIL) process, as schematically illustrated in Figure 2a. The CAN microspheres were deposited onto a Si wafer (containing a native oxide layer) using a dip-coating process. Differently sized, nondeformable silica particles were co-deposited and functioned as spacers during the UV-NIL process. A transparent, untreated glass slide with no notable UV absorption (Glass Microscope Slide, Corning) was used as superstrate to apply a compressive loading on the particles while allowing UV penetration (300–400 nm wavelength at a 20 mW/cm^2 intensity, measured through the glass slide, is used throughout). In this work, the pressure applied to the confining glass slide/wafer was fixed at 3 MPa, but the true pressure on each particle should be at least 2 orders of magnitude higher since the surface coverage of the particles was low (estimated to be <1% from Figure S5). The use of rigid silica spacers between the CAN particles limits the upper bound on the strain that is achieved. Given a true pressure >100 MPa applied to the particles, we assume the imprinting conditions are able to compress the particles down to the height of the silica spacers, allowing for stress–relaxation experiments under compressive loading. After UV irradiation, the pressure was released, and the resultant particle shapes were characterized.

Figure 2b presents the side-view scanning electron microscopy (SEM) images of the CAN particles before and after 15 min of UV irradiation in the presence of 0.73 μm silica spacers. The microspheres were successfully reconfigured into a permanent, nonspherical shape. The particles in both images exhibited distinctive surface wrinkles, which were induced by the focused electron beam and could not be avoided during side-view imaging (see Supporting Information for discussion, Figure S4). Although this e-beam induced surface-wrinkling could be chemical-specific and a unique way to create the particle surface morphology, it prevents reliable characterization of the particle geometry. Instead, we applied AFM to quantify the particle shapes for all subsequent studies. Specifically, the shape of the oblate ellipsoidal particles is represented by the width (w) and height (h), which are determined from AFM measurements.

First, we examined the influence of UV irradiation time on the degree of particle shape reconfiguration. Particles were subject to a fixed, elastic, compressive prestrain, $\varepsilon_E = 0.76$, obtained using 0.73 μm silica spacers. As a control, when no UV exposure was performed during compression, particles returned to an aspect ratio of ~1.1 upon pressure release. The inability of particles to fully return to their initial spherical shape, in the absence of any network reconfiguration, is consistent with our recent study on the influence of particle–

substrate adhesion following particle compression.[37] Compressed particles were then exposed to UV irradiation for different durations. As summarized in Figure 2c, the aspect ratio w/h of the resultant CAN particles increased from 1.2, 2.1, 2.8, to 3.4 as UV irradiation increased from 1, 5, 10, to 15 min, respectively. These values are all larger than the aspect ratio of the control trial, suggesting that the final particle shape was dominated by RAFT-mediated stress relaxation within the particles, rather than particle–substrate adhesion.

To better quantify the degree of shape configuration for the CAN particles, we define

$$\text{fixity} = \frac{\varepsilon_F}{\varepsilon_E} \times 100\%$$

where ε_E is the initial strain of the compressed particle (defined by the size of the silica spacer), and ε_F is the final (or permanent) strain achieved after the UV-NIL process. The fixity describes the percentage of the initial elastic strain that was converted into permanent strain due to the network rearrangement. Accordingly, fixity for vertical and lateral directions increases with the UV irradiation time (Figure 2c). However, the fixity was larger for the particle height than for the width, which is an inherent feature for compressive deformation of spheres. For a rubbery sphere, at large compressive strains, small changes in particle height are accompanied by larger changes in particle width. For example, when the particle height changes from a compressive strain of $\varepsilon_E = 0.76$ to $\varepsilon_F = 0.46$, i.e., a 60% height fixity, the corresponding width fixity is only 23%.

Without question, the degree of particle shape reconfiguration is directly attributed to the degree of stress relaxation of the polymer network. Directly measuring the degree of stress relaxation during UV-NIL within a compressed CAN microparticle is challenging. Instead, we developed a finite element model (FEM) to simulate the recovered particle shape after the UV-NIL process (assumes no substrate adhesion, see Supporting Information for more info), which allows us to estimate the degree of stress relaxation. Most significantly, the degree of stress relaxation is quantified as $\sigma_t = f\sigma_0$, where σ_0 is the Cauchy stress in the compressed particle before UV irradiation, and f denotes the stress relaxation ratio and is set to be uniform within the particle.[38,39] With a fit of the experimentally measured particle aspect ratio, the degree of stress relaxation f was extracted. As summarized in Figure 2d, the degree of stress relaxation increases with an increase of the UV irradiation time, nearing a steady state of ~50% after 15 min.

Figure 2d displays the shape as well as the residual stress state of the reconfigured particles, obtained from the FEM. Full-shape imaging with SEM and AFM was challenged by the chemical stability and AFM tip–particle convolution, correspondingly. The simulated shape provides a full view of the particle. In addition, the residual stress within the reconfigured particles was evident, particularly for the longer UV exposure times. From FEM, this residual stress is inherent to CANs with partial stress relaxation (in our 50% MBTA system): There is competition between the unrelaxed network chains and the chains that were relaxed during UV-NIL. The lowest energy state of the former is the original spherical shape, while the latter energetically favors the compressed shape imposed during UV-NIL. The final

particle shape therefore results from a balance between the two types of network strands. If the residual stress were completely eliminated, then 100% fixity would be expected.

Next, we examined the influence of ε_E on the degree of shape reconfiguration (Figure 2e) and the corresponding degree of stress relaxation (Figure 2f). The CAN particles were compressed to varying ε_E using differently sized silica spacers, and then irradiated with UV light for 15 min. As summarized in Figure 2e, the aspect ratios of the reconfigured particles were 1.3, 2.3, and 3.4, with ε_E = 0.37, 0.69, and 0.76, respectively. A larger degree of shape reconfiguration in CAN particles was achieved with larger ε_E. Interestingly, the fixity value for particle height appears to be lower than that for particle width for ε_E = 0.37, while the opposite was observed for ε_E = 0.69 and 0.76. This behavior is attributed to the unique geometric constraints for compressed spheres: at low degrees of compression (ε_E < ~0.5), the vertical deformation ratio is larger than that of the lateral expansion; at higher degree of compression (ε_E > ~0.5), the opposite trend is true.

Using FEM, the degree of stress relaxation in the CAN particles was estimated to be ~42% for ε_E = 0.37 and 0.69, and ~49% for ε_E = 0.76, respectively (Figure 2f). The higher degree of stress relaxation at ε_E = 0.76 is intriguing, which might indicate the stress relaxation is strain-dependent, especially at the high strain level. Nonetheless, the degree of stress relaxation in all samples agrees well with the percentage of the RAFT-agent (50%), suggesting that the majority of the active bonds participated in the network rearrangement process. The full shapes of the corresponding reconfigured particles were simulated from the FEM (inset of Figure 2f). Accordingly, the FEM also suggests that the residual stress in the reconfigured CAN particles increases with an increase of ε_E, due to the redeformation of the already relaxed chains during particle recovery.

The use of UV-NIL to reconfigure the shapes of CAN-based particles is attractive because it allows further lithographic control over the particle surface features. To demonstrate this feature, we used a patterned Si mold (1:1 line-space grating pattern, with an 840 nm periodicity and a groove depth of 200 nm) as the supporting substrate for the particle shape-reconfiguration process using the UV-NIL. Figure 3a shows the AFM images of a CAN particle after 15 min UV irradiation under a 3 MPa pressure with the use of 0.73 μm spacers. The aspect ratio of the particle is 3.4, consistent with Figure 2e, and the average pattern height replicated on the particle surface was 100 nm. This pattern height represents ~50% of the mold depth, consistent with the degree of partial stress relaxation shown in Figure 2f.

AFM may also be employed to directly write features on the surface of CAN particles. This concept is demonstrated in Figure 3b,c where indentations having depths of 220 and 20 nm, respectively, have been imposed on the surface without significantly altering the larger aspect ratio. These indentations are achieved by pushing the AFM tip into the as-deposited CAN particle and exposing the sample to the Bluedrive laser built into the AFM (360–410 nm wavelength, magnitude of irradiance is unknown) for 30 s (see Supporting Information for more details, Figure S5). The indentation in Figure 3b is hundreds of nanometers deep and is observed to remain on the particle surface after an additional 30 s of UV exposure without AFM loading. Figure 3c, however, shows an indentation only 20 nm deep (center, cross-section in Supporting Information Figure S6) which is then erased after exposure to

the Bluedrive laser for an additional 30 s without AFM loading (bottom). The size of this smaller indentation is very close to the elastocapillary length scale of the particle (~10 nm), so when stress relaxation is initiated in the absence of AFM loading, the Laplace pressure may be great enough to deform and erase the feature. We expect that Laplace pressure, in the absence of AFM loading, would also be able to smooth out the larger surface features in Figure 3a,b if covalent bond exchange were to continue for time scales significantly larger than those achieved in this work.

In conclusion, this work demonstrated the light-stimulated permanent shape reconfiguration of polymer microspheres based on novel covalent adaptive network chemistry. Using RAFT-based chemistry as a model system, we showed that CAN microspheres can be reconfigured into a series of oblate ellipsoidal particles with aspect ratios as high as 3.4 using a UV-NIL setup. With adjustment of the UV-NIL process conditions including UV irradiation time and prestrain, the degree of stress relaxation within the CAN particles is readily controlled, which results in different degrees of shape reconfiguration. The use of UV-NIL allows programming of complex topographies onto CAN particle surfaces by using either topographic molds or AFM indentation. This approach provides a platform to custom fabricate unique nonspherical polymer particles with geometric complexity beyond the capabilities of current top-down lithographic techniques. The FEM methods developed here further allow predictive control over the final particle shape.

MATERIALS AND METHODS

RAFT-based microparticles were synthesized as follows. In a 20 mL drum vial, pentaerythritol tetrakis(3-mercaptopropionate) (PETMP, 244 mg, 2 mmol of thiol group), tetra(ethylene glycol) diacrylate (TEGDA 151 mg, 1 mmol of acrylate group), 2-methylene-propane-1,3-bis(thioethyl acrylate) (MBTA, 158 mg, 1 mmol of acrylate group), polyvinylpyrrolidone(PVP, 276 mg, 50 wt % to monomers), and the photoinitiator Irgacure 651 (5.53 mg, 1 wt % to monomers) were dissolved in 10 mL of methanol, and a clear yellowish solution was obtained. MBTA was synthesized according to the literature.[34] Under vigorous magnetic stirring, 76 μL of triethylamine (10 wt % to monomers) was added; the mixture immediately turned turbid, and a stable dispersion was generated. The reaction was allowed to continue stirring for 1 h before the microparticles were harvested by centrifuge and washed with methanol three times.

Infrared spectroscopy (IR, Thermo Nicolet 670) measurements were performed on the CAN particles. No residual, unreacted polymerizable functional groups remained in the particles, indicating that the bond-exchanging allyl sulfide compound contained in the MBTA monomer had been successfully integrated into the network. The diameter of the unswollen particles was measured via AFM (DI 3100, Bruker) to be 3.1 μm ± 0.3 μm (n = 30); this narrow polydispersity is consistent with existing literature.[35,36] The particles were also imaged in top-down and side-view mode using an FE-SEM (Zeiss, Supra 60). Prior to SEM imaging, the deposited particles were sputter-coated with an approximately 5 nm layer of gold.

Force–displacement curves employing an AFM probe tip with a 60 nm diameter hemispherical apex (HSC60 225C3/MC/R, Team Nanotech), coated with a metal carbide film to reduce tip wear, was employed in a Cypher AFM (Asylum) to directly measure the Young's modulus of the particles. Applying a JKR model to the force curves yields a modulus of 10 MPa. AFM imprinting of surface topography was performed on the Cypher AFM using an AFM probe tip (CONTATEC, AdvanceTec) that protrudes out from the end of the cantilever, allowing top-down illumination of the tip–sample contact region.

Films with a similar chemical composition were synthesized between glass slides using spacers to maintain a constant thickness. Dynamic mechanical analysis (TA Q800) measurements were carried out on samples with approximately 10 mm × 5 mm × 0.25 mm ($L \times W \times T$) to determine the T_g and temperature dependence of the mechanical properties. The measurements were taken from −50 to 30 °C at a rate of 3 °C/min, under a strain amplitude of 0.1%.

Silica spacers with diameters of 0.73, 0.98, and 1.95 μm were mixed into separate methanol solutions containing polymer particles. Droplets of the solutions were then dispersed onto silicon wafers and dried in a vacuum desiccator for 1 h. Next, particles were compressed between two parallel plates via NIL (Eitre 3, Obducat). In this case, one of the two plates is the substrate upon which particles were deposited, and the other plate is a transparent glass slide to allow for transmission of UV light (300–400 nm at an intensity of 20 mW/cm^2). All NIL processes were performed and released at 40 °C, under a pressure of 3 MPa, with the UV light source illuminating the samples for various durations.

Supplementary Material

Refer to Web version on PubMed Central for supplementary material.

Acknowledgments

We would like to acknowledge the funding support from the National Science Foundation under Grants CMMI-1233626, CBET-1264276, and DMR-1310528, as well as funding from the National Institute of Health under Grant 1U01DE023777-01. X.S. and H.-A.W. acknowledge support from the National Natural Science Foundation of China (11525211) and the Strategic Priority Research Program of the Chinese Academy of Sciences (XDB22040502). R.L. acknowledges the support from of the Ralph E. Powe Junior Faculty Enhancement award from Oak Ridge Associated Universities (ORAU). Publication of NIST, an agency of the US government, not subject to copyright. Certain commercial equipment, instruments, or materials are identified in this paper in order to specify the experimental procedure adequately. Such identification does not imply recommendation or endorsement by NIST, nor does it imply that the materials or equipment identified are necessarily the best available for the purpose.

References

1. Yeo SJ, Park KJ, Guo K, Yoo PJ, Lee S. Microfluidic Generation of Monodisperse and Photoreconfigurable Microspheres for Floral Iridescence–Inspired Structural Colorization. Adv Mater. 2016; 28:5268–5275. [PubMed: 27153473]
2. Lu Y, Yin Y, Xia Y. Three-Dimensional Photonic Crystals with Non-Spherical Colloids as Building Blocks. Adv Mater. 2001; 13:415–420.
3. Hardy JG, Palma M, Wind SJ, Biggs MJ. Responsive Biomaterials: Advances in Materials Based on Shape-Memory Polymers. Adv Mater. 2016; 28:5717–5724. [PubMed: 27120512]

4. He Y, Park K. Effects of the Microparticle Shape on Cellular Uptake. Mol Pharmaceutics. 2016; 13:2164–2171.
5. Li M-C, Wu Q, Song K, Qing Y, Wu Y. Cellulose Nanoparticles as Modifiers for Rheology and Fluid Loss in Bentonite Water-Based Fluids. ACS Appl Mater Interfaces. 2015; 7:5006–5016. [PubMed: 25679499]
6. Fu S-Y, Feng X-Q, Lauke B, Mai Y-W. Effects of Particle Size, Particle/Matrix Interface Adhesion and Particle Loading on Mechanical Properties of Particulate–polymer Composites. Composites, Part B. 2008; 39:933–961.
7. Ahmed S, Jones FR. A Review of Particulate Reinforcement Theories for Polymer Composites. J Mater Sci. 1990; 25:4933–4942.
8. Li J, Mazumder MAJ, Stöver HDH, Hitchcock AP, Shirley IM. Polyurea Microcapsules: Surface Modification and Capsule Size Control. J Polym Sci, Part A: Polym Chem. 2011; 49:3038–3047.
9. Takekoh R, Li W-H, Burke NAD, Stöver HDH. Multilayered Polymer Microspheres by Thermal Imprinting during Microsphere Growth. J Am Chem Soc. 2006; 128:240–244. [PubMed: 16390152]
10. Zhao Y, Burke NAD, Stöver HDH. Structured Poly(divinylbenzene-Co-Chloromethylstyrene) Microspheres by Thermal Imprinting Precipitation Polymerization. J Polym Sci, Part A: Polym Chem. 2016; 54:1159–1166.
11. Lebre F, Hearnden CH, Lavelle EC. Modulation of Immune Responses by Particulate Materials. Adv Mater. 2016; 28:5525–5541. [PubMed: 27167228]
12. Yang Z, Huck WTS, Clarke SM, Tajbakhsh AR, Terentjev EM. Shape-Memory Nanoparticles from Inherently Non-Spherical Polymer Colloids. Nat Mater. 2005; 4:486–490. [PubMed: 15895098]
13. Wischke C, Schossig M, Lendlein A. Shape-Memory Effect of Micro-/Nanoparticles from Thermoplastic Multiblock Copolymers. Small. 2014; 10:83–87. [PubMed: 23847123]
14. Cox LM, Killgore JP, Li Z, Zhang Z, Hurley DC, Xiao J, Ding Y. Morphing Metal–Polymer Janus Particles. Adv Mater. 2014; 26:899–904. [PubMed: 24167094]
15. Bowman CN, Kloxin CJ. Covalent Adaptable Networks: Reversible Bond Structures Incorporated in Polymer Networks. Angew Chem, Int Ed. 2012; 51:4272–4274.
16. Rowan SJ, Cantrill SJ, Cousins GRL, Sanders JKM, Stoddart JF. Dynamic Covalent Chemistry. Angew Chem, Int Ed. 2002; 41:898–952.
17. Kloxin CJ, Bowman CN. Covalent Adaptable Networks: Smart, Reconfigurable and Responsive Network Systems. Chem Soc Rev. 2013; 42:7161–7173. [PubMed: 23579959]
18. Montarnal D, Capelot M, Tournilhac F, Leibler L. Silica-Like Malleable Materials from Permanent Organic Networks. Science. 2011; 334:965–968. [PubMed: 22096195]
19. Taynton P, Yu K, Shoemaker RK, Jin Y, Qi HJ, Zhang W. Heat- or Water-Driven Malleability in a Highly Recyclable Covalent Network Polymer. Adv Mater. 2014; 26:3938–3942. [PubMed: 24677455]
20. Amamoto Y, Kamada J, Otsuka H, Takahara A, Matyjaszewski K. Repeatable Photoinduced Self-Healing of Covalently Cross-Linked Polymers through Reshuffling of Trithiocarbonate Units. Angew Chem. 2011; 123:1698–1701.
21. Berg GJ, Gong T, Fenoli CR, Bowman CN. A Dual-Cure, Solid-State Photoresist Combining a Thermoreversible Diels–Alder Network and a Chain Growth Acrylate Network. Macromolecules. 2014; 47:3473–3482.
22. Adzima BJ, Aguirre HA, Kloxin CJ, Scott TF, Bowman CN. Rheological and Chemical Analysis of Reverse Gelation in a Covalently Cross-Linked Diels–Alder Polymer Network. Macromolecules. 2008; 41:9112–9117. [PubMed: 20711364]
23. Otsuka H, Nagano S, Kobashi Y, Maeda T, Takahara A. A Dynamic Covalent Polymer Driven by Disulfide Metathesis under Photoirradiation. Chem Commun. 2010; 46:1150–1152.
24. Wojtecki RJ, Meador MA, Rowan SJ. Using the Dynamic Bond to Access Macroscopically Responsive Structurally Dynamic Polymers. Nat Mater. 2011; 10:14–27. [PubMed: 21157495]
25. Scott TF, Schneider AD, Cook WD, Bowman CN. Photoinduced Plasticity in Cross-Linked Polymers. Science. 2005; 308:1615–1617. [PubMed: 15947185]

26. Cox LM, Li Z, Sowan N, Nair D, Xiao J, Bowman CN, Ding Y. Reconfigurable Surface Patterns on Covalent Adaptive Network Polymers Using Nanoimprint Lithography. Polymer. 2014; 55:5933–5937.
27. Fenoli CR, Wydra JW, Bowman CN. Controllable Reversible Addition–Fragmentation Termination Monomers for Advances in Photochemically Controlled Covalent Adaptable Networks. Macromolecules. 2014; 47:907–915.
28. Leung D, Bowman CN. Reducing Shrinkage Stress of Dimethacrylate Networks by Reversible Addition–Fragmentation Chain Transfer. Macromol Chem Phys. 2012; 213:198–204.
29. Kloxin CJ, Scott TF, Bowman CN. Stress Relaxation via Addition–Fragmentation Chain Transfer in a Thiol-Ene Photopolymerization. Macromolecules. 2009; 42:2551–2556. [PubMed: 20160931]
30. Zhang B, Wang X, Zhu A, Ma K, Lv Y, Wang X, An Z. Enzyme-Initiated Reversible Addition–Fragmentation Chain Transfer Polymerization. Macromolecules. 2015; 48:7792–7802.
31. Park HY, Kloxin CJ, Scott TF, Bowman CN. Covalent Adaptable Networks as Dental Restorative Resins: Stress Relaxation by Addition–fragmentation Chain Transfer in Allyl Sulfide-Containing Resins. Dent Mater. 2010; 26:1010–1016. [PubMed: 20655100]
32. Yang H, Yu K, Mu X, Shi X, Wei Y, Guo Y, Qi HJ. A Molecular Dynamics Study of Bond Exchange Reactions in Covalent Adaptable Networks. Soft Matter. 2015; 11:6305–6317. [PubMed: 26166382]
33. Jin K, Li L, Torkelson JM. Recyclable Crosslinked Polymer Networks via One-Step Controlled Radical Polymerization. Adv Mater. 2016; 28:6746–6750. [PubMed: 27206061]
34. Kloxin CJ, Scott TF, Park HY, Bowman CN. Mechanophotopatterning on a Photoresponsive Elastomer. Adv Mater. 2011; 23:1977–1981. [PubMed: 21360784]
35. Wang C, Zhang X, Podgórski M, Xi W, Shah P, Stansbury J, Bowman CN. Monodispersity/Narrow Polydispersity Cross-Linked Microparticles Prepared by Step-Growth Thiol–Michael Addition Dispersion Polymerizations. Macromolecules. 2015; 48:8461–8470.
36. Wang C, Zieger MM, Schenzel A, Wegener M, Willenbacher J, Barner-Kowollik C, Bowman CN. Photoinduced Tetrazole-Based Functionalization of Off-Stoichiometric Clickable Microparticles. Adv Funct Mater. 2017; 27:1605317.
37. Cox LM, Killgore JP, Li Z, Long R, Sanders AW, Xiao J, Ding Y. Influences of Substrate Adhesion and Particle Size on the Shape Memory Effect of Polystyrene Particles. Langmuir. 2016; 32:3691–3698. [PubMed: 27023181]
38. Long R, Qi HJ, Dunn ML. Thermodynamics and Mechanics of Photochemcially Reacting Polymers. J Mech Phys Solids. 2013; 61:2212–2239.
39. Long KN, Scott TF, Qi HJ, Bowman CN, Dunn ML. Photomechanics of Light-Activated Polymers. J Mech Phys Solids. 2009; 57:1103–1121.

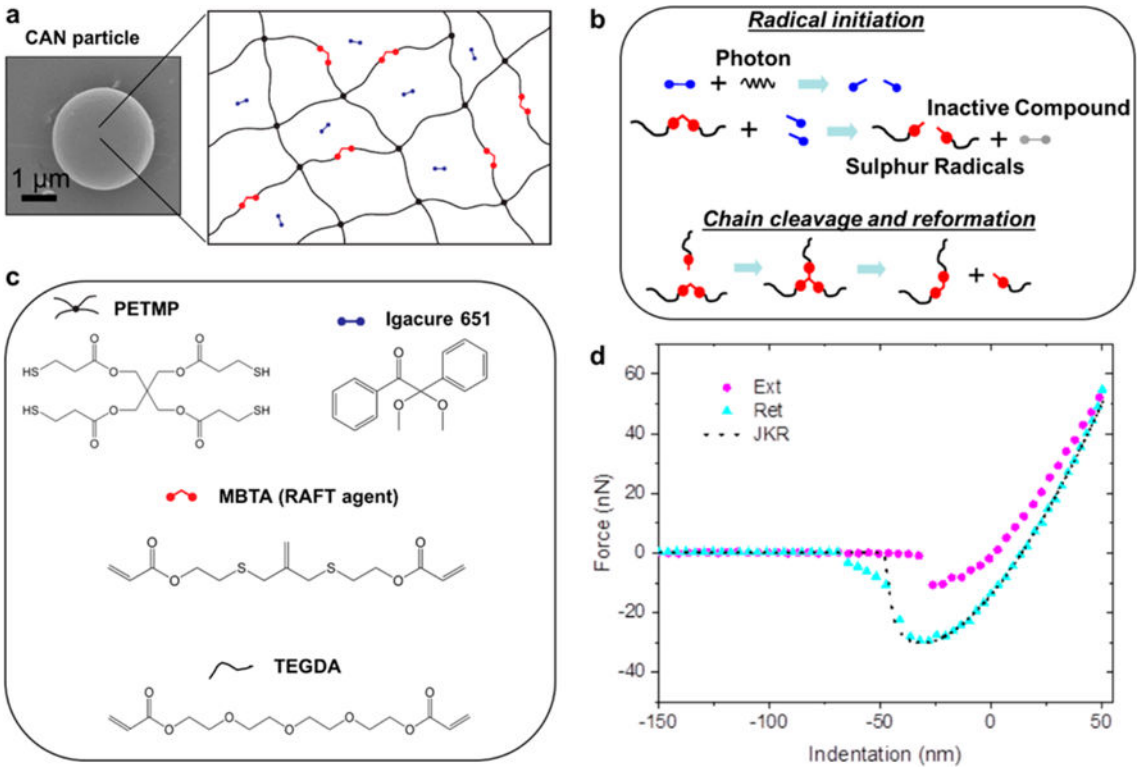

Figure 1.

(a) SEM image of an as-prepared CAN microsphere and an illustration of different components in the network structure. (b) Illustration of the radical-mediated RAFT-based bond-exchange process. (c) Chemical formula of the monomers, cross-linkers including RAFT-agent containing monomer, and photoinitiator used in the synthesis of the CAN particle networks as shown in part a. (d) AFM-indentation measurements and associated mechanical behavior of a single CAN particle at ambient temperature. The data points are the experimental results, and the dotted line shows the theoretical retraction profile of a Johnson Kendall Roberts (JKR) contact model for a rubbery particle with a 12 MPa modulus.

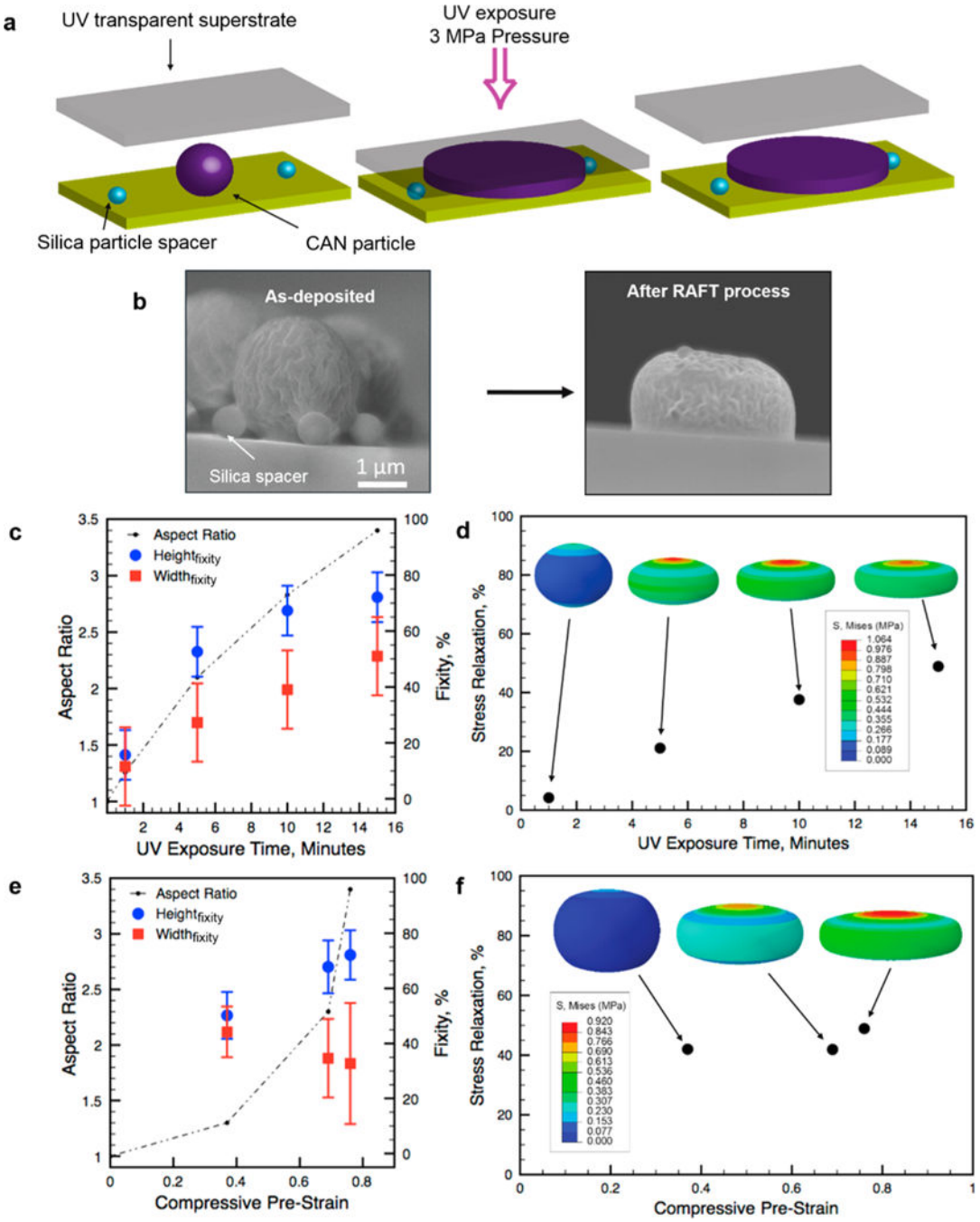

Figure 2.

(a) Schematic of particle reconfiguration using UV-NIL. (b) Side-view SEM images of particles before (left) and after (right) UV-NIL (15 min of UV irradiation with 0.73 μm silica spacers), scale bar applies to both images. (c). Aspect ratio (line) between particle width and height of the particles after UV-NIL as a function of UV exposure time, as well as shape fixity of the height (●) and width (■). (d) Degrees of stress relaxation, for each exposure time, obtained by inputting AFM measured aspect ratios into the FEM. Also shown are FEM-simulated particle shapes and residual stress distributions within the reconfigured

particles. (e) Aspect ratio (line) after UV-NIL as a function of prestrain, as well as shape fixity of the height (●) and width (■). (f) Stress relaxation and corresponding FEM-simulated particle shapes for each compressive prestrain.

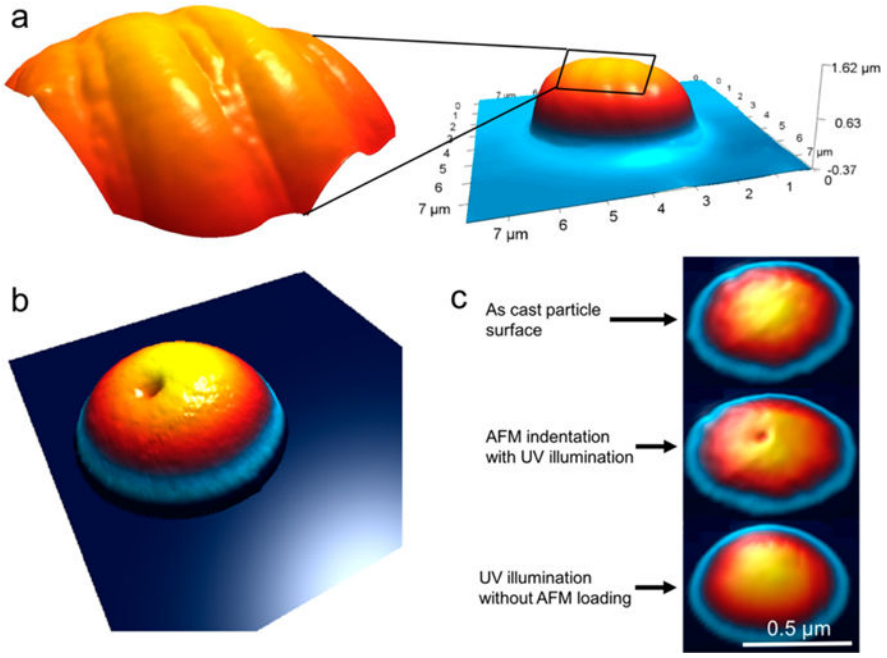

Figure 3.

(a) AFM scans of particles imprinted using a silicon mold with a line-space grating pattern. 0.73 μm spacers were used to control vertical deformation. (b) AFM scans of an as-deposited CAN particle, after 1 min AFM indentation with blue LED illumination yields an indentation 220 nm deep. (c) A small, 20 nm deep indentation is imposed on a particle surface after 15 s of irradiation and AFM indentation. It is observed to disappear after another 30 s with blue-laser irradiation without AFM loading (right).